Electrochimica Acta 154 (2015) 278–286

Contents lists available at ScienceDirect

Electrochimica Acta

journal homepage: www.elsevier.com/locate/electacta

Insights into electrodegradation mechanism of tebuconazole pesticide on Bi-doped PbO_2 electrodes

Francisco de Assis Avelino de Figueredo-Sobrinho [a], Francisco Willian de Souza Lucas [b], Taicia Pacheco Fill [b], Edson Rodrigues-Filho [b], Lucia Helena Mascaro [b], Paulo Naftali da Silva Casciano [a], Pedro de Lima-Neto [a], Adriana Nunes Correia [a,*]

[a] Departamento de Química Analítica e Físico-Química, Centro de Ciências, Universidade Federal do Ceará, Bloco 940 Campus do Pici, 60440-900 Fortaleza-CE, Brazil
[b] Departamento de Química, Universidade Federal de São Carlos, Caixa Postal 676, 13565-905, São Carlos-SP, Brazil

ARTICLE INFO

Article history:
Received 6 October 2014
Received in revised form 27 November 2014
Accepted 10 December 2014
Available online 11 December 2014

Keywords:
Bi-doped PbO_2
Electrodegradation
Tebuconazole
HPLC–ESI/HRMS
Oxidation pathway

ABSTRACT

The effect of the Bi doping of PbO_2 coatings on the electrochemical degradation of the pesticide tebuconazole (TBC) was investigated. The insertion of 8% Bi (relative to the amount of Pb) in the PbO_2 structure afforded a well-defined texturing in the direction of the (2 0 0) plane to the PbO_2 coatings, as well as, a decrease in the size of the coherent domain of the crystal, an increase in the electrochemical roughness and in the oxidation power of the Bi-doped PbO_2 compared with PbO_2. Through ultraviolet-visible spectrometry and total organic carbon (TOC) analyses for TCB electrodegradation was possible to chose the current density of 40 mA cm^{-2} as optimized one, with 68% of TOC removed by the Bi-doped electrode and 56% removed by the PbO_2 electrode. High resolution liquid chromatography coupled with electrospray ionisation high resolution mass spectrometry helped to propose an oxidation pathway for the electrochemical degradation of TBC. Nine electrooxidation products were identified; which were produced by hydroxylation of the TBC phenyl group and its consequent oxidation to a ketone (including both mono- and dihydroxylated products), by dechlorination (two different products), and by multiple oxidative steps with ring opening (two different products). It was possible to conclude that the electrooxidation of TBC using Bi-doped PbO_2 anodes generated products that were less harmful than TBC itself, thus recommending this electrode as an alternative material for wastewater decontamination.

1. Introduction

In recent years, the increasing focus on environmental sustainability has led to more stringent laws with the aim of minimising the levels of effluent pollution. Correspondingly, research and development into more efficient, alternative technologies to enable wastewater treatment, without causing further environmental damage, has grown. Industrial wastes are complex and usually consist of organic and inorganic compounds, which make the treatment processes more difficult because there is not universal treatment strategy. For effluents contaminated with organic compounds, the most economically viable alternative treatment is biological oxidation, although some toxic or biorefractory molecules are not appropriately decomposed by this method. Other methods used for industrial effluent decontamination, such as physicochemical methods, chemical oxidation and advanced oxidation processes (AOP), also have some disadvantages, such as the utilisation and transportation of strong oxidising chemicals and the generation of sludge or toxic byproducts [1–3].

In this context, electrochemical oxidation technologies represent an economically and environmentally viable alternative, where the main reagent is the electron, which is versatile, efficient, cost-effective and clean [2,4]. Electrochemical degradation methods have been widely used for the decontamination of wastewater polluted with dyes, pharmaceuticals and pesticides [2,5,6]. We focused on pesticides because these compounds are very harmful to the environment and to human health [7,8]. Most such compounds are not biodegradable because of their very stable molecular structures; thus, their residues can remain in the soil, contaminating crops and natural waterways and impacting aquatic life. From among this emerging class of contaminants, tebuconazole (TBC) pesticide attracted our attention because of its high photochemical stability; its photodegradation in soil (under

* Corresponding author. Tel.: +55 85 3366 9050.
E-mail address: adriana@ufc.br (A.N. Correia).

http://dx.doi.org/10.1016/j.electacta.2014.12.062
0013-4686/

natural sunlight) occurs slowly. It has been observed that 86% of the parent compound remains after 34 days of irradiation, and no photoreaction occurs in aqueous solution after 30 days of irradiation [9]. Furthermore, according to Götz et al. [10], it exhibits a high likelihood of occurrence in surface waters [11]. This pesticide has been detected in several influent and effluent sources, e.g., headwaters and ditches [12,13], in small lowland streams in the region of Braunchweig (Northern Germany) [13], in effluents of wastewater treatment plants in Lyon (St. Fons, France) and in Marburg (Hessen, Germany) [14,15]. This pesticide has also been detected in rainwater samples in the Trier region (Germany) at concentrations of 12–187 ng L^{-1} [16].

Tebuconazole, [(RS)-1-p-chlorophenyl-4,4-dimethyl-3-(1H-1,2,4-triazol-1-ylmethyl) pentan-3-ol], belongs to the triazole fungicide class, one of the major classes of pesticides that is widely used in agriculture. In Brazil, this fungicide is allowed on 42 types of crops by National Health Surveillance Agency (ANVISA) [17]. There has been no research into the electrochemical degradation of this pesticide or the products generated during this degradation. There are only a few works concerning its photocatalytic degradation [18,19], and one proposition of products generated by its photodegradation [20]. Navarro et al. [18] described the photomineralisation of this pesticide using ZnO as photocatalyst, obtaining good results with complete mineralisation in 2 h. However, they used $Na_2S_2O_8$ as oxidant, which will remain in the solution as a chemical waste and, moreover, they did not evaluate the formed byproducts. Prestes et al. [19] studied the photodegradation of the TBC using TiO_2 as photocatalyst; nevertheless, they did not determine the total organic carbon removal or the formed byproducts. The photodegradation products of the TBC were evaluated by Calza et al. [20]. They used a high-performance liquid chromatographic/tandem mass spectrometry to identify these products, but they did not study the degradation efficiency.

Concerning the electrochemical degradation of tebuconazole, also a type of AOP, the major oxidising species are the hydroxyl radicals, which are generated from the oxidation of water. One of the main factors determining the efficiency of the decontamination process is the electrode surface. The known dimensionally stable anodes (DSA) [21] are widely used in the industrial production of chlorine and alkali compounds from the electrolysis of seawater and have been used for the electrochemical oxidation of organic compounds in wastewater processes [22–24].

DSAs, such as Pt, Ti/TiO_2-RuO_2 and Ti/TiO_2–IrO_2, are used for the electrodegradation of emerging contaminants and are known as active electrodes. In these cases, hydroxyl radicals (•OH) are strongly bound to the electrode surface by chemisorption; consequently, the oxidation of organic compounds is less efficient. For non-active electrodes, hydroxyl radicals are weakly adsorbed to the electrode surface by physisorption, resulting in higher electrochemical degradation efficiency for organic compounds than for the above-mentioned active electrodes. Some examples of non-active electrodes are Ti/PbO_2, Ti/SnO_2–Sn_2O_5 and p-Si/boron-doped diamond. Of these, we focused on Ti/PbO_2 because of its low cost (in comparison to noble metal electrodes), high electrical conductivity, large overpotential for the oxygen evolution reaction (OER) and high physical and chemical stability under controlled conditions, all of which makes it applicable in various processes [2,25].

Lead dioxide has attracted considerable attention due to its use as the active material in the positive plate of the lead-acid cell [25]. Several applications for this electrode are reported in the literature, including oxygen and ozone production by water electrolysis, the manufacture of chemicals and water effluent treatment [25]. PbO_2 is polymorphic, with two well-known phases: α-PbO_2, with the orthorhombic structure of columbite, and β-PbO_2, with a tetragonal rutile structure. Some studies have shown that the inclusion of certain species in PbO_2 coatings can cause modifications of their electrocatalytic and mechanical properties [25]. The literature indicates that the incorporation of ions such as Bi^{3+}, Bi^{5+}, Fe^{3+}, Co^{2+} and F^-improves stability and electrocatalytic activity, making a more effective surface for oxygen transfer reactions, including O_3 formation, that are associated with degradation of contaminants [26–28]. Bi-doped PbO_2 electrodes have been shown to catalyse the oxidation of inorganic ions and the removal of total organic carbon (TOC) and to reduce fouling by organics [25]. Studies have indicated that the Bi-doped PbO_2 electrode is more mechanically stable and has a higher electrocatalytic activity compared with the PbO_2 electrode [29,30].

The aim of this paper is to evaluate the effect of Bi insertion in electrodeposited PbO_2 coatings on Ti/SnO_2-Sb_2O_5 and to analyse the applicability of the resulting electrode in the TBC electrodegradation, identify the formed products by high resolution liquid chromatography coupled with electrospray ionisation high-resolution mass spectrometry (HPLC–ESI/HRMS) and propose the oxidation mechanism of TBC.

2. Experimental

2.1. Chemicals

Tebuconazole (Sigma–Aldrich, CAS No. 107534-96-3) was used as received. All other chemicals were of analytical grade. All solutions were prepared with Millipore Waters deionised water (18.2 MΩ cm^{-1} at 25 °C) and were prepared prior to use.

2.2. Apparatus

The electrodeposition of PbO_2 and Bi-doped PbO_2 coatings, as well as all electrochemical experiments, were performed using a potentiostat/galvanostat (Autolab PGSTAT30, Metrohm-Eco Chemie, The Netherlands) controlled by the GPES 4.9 software. A three-electrode electrochemical cell with a volume of 100 mL was used. The electrodeposition substrate, i.e., the film to be studied (1.5 cm^2 of geometric area), was used as the working electrode, a Pt plate (4 cm^2 geometric area) as the auxiliary electrode and an Ag/AgCl/saturated KCl as the reference electrode.

The composition and morphology of the Ti/SnO_2–Sb_2O_5 (substrate), PbO_2 and Bi-doped PbO_2 films were evaluated by high-resolution field emission scanning electron microscopy (FE-SEM, Zeiss Supra 35 at 2 kV) and by energy dispersive X-ray (EDX) spectroscopy (FEI XL30 FEG with an Oxford Instruments-Link ISIS 300 detector), respectively.

PbO_2 and Bi-doped PbO_2 films were characterised by X-ray diffraction (XRD), which was performed using a X-ray diffractometer (Rigaku-D/Max 2500PC) with CuKα radiation, a scanning step of 0.02°, a counting time of 6 s and a 2θ range from 20° to 80° at 27 °C. The size of the coherent domain of the crystal (*D*, nm) was estimated from the (1 0 1) β-PbO_2 peak using the Scherrer equation, where line broadening from instrumental effects was corrected using the Caglioti equation with a Silicon powder standard (99%, 325 mesh, SRM-640), as described by Gonçalves et al. [31]. All samples were refined by the Rietveld method [32] using the GSAS program [33]. The input data for the theoretical model were taken from the Inorganic Crystal Structure Database (ICSD) [34].

The electrodegradation was monitored by ultraviolet-visible spectrometry, using a UV–vis spectrophotometer (Cary 5G, Varian), and by total organic carbon (TOC) measurements, using a Shimadzu TOC-L apparatus.

The electrochemical oxidation mechanism was studied using high-resolution liquid chromatography coupled with electrospray

ionisation high-resolution mass spectrometry (HPLC–ESI/HRMS), carried out on a LTQ-Orbitrap Thermo Fisher Scientific mass spectrometry system (Bremen, Germany), with the resolution set at 60 K. The Thermo Scientific HPLC was fitted with a 5 μ phenyl-hexyl column (4.6 × 250 mm, Phenomenex), and samples were eluted using a linear gradient, ranging from 50% to 90% acetonitrile in water over 30 min, at a flow rate of 0.7 mL min^{-1}.

2.3. Preparation and characterisation of the electrodes

PbO_2 and Bi-doped PbO_2 coatings were electrodeposited on Ti plates (3 × 1.5 × 0.05 cm, from TiBrasil Titânio Ltda.) with an oxide interlayer of SnO_2–Sb_2O_5 formed by thermal decomposition. The Ti plates were degreased with acetone, etched in a boiling 10% oxalic acid solution for 1 h and rinsed with distilled water. Ti/SnO_2–Sb_2O_5 substrates were prepared using a solution containing 8.5 g $SnCl_4$ (Aldrich) and 5.0 g $SbCl_3$ (Fluka) dissolved in a mixture of 40 mL n-butanol (Merck) with 10 mL of concentrated HCl (Merck). The precursor solution was painted onto Ti plates with a brush, after which the material was thermally treated at 130 °C for 10 min to eliminate part of the solvent and then at 400 °C for 10 min to improve film adherence. This procedure was repeated 20 times. Finally, the film was treated at 600 °C for 1 h to eliminate the organic portion, leading to the metal oxide film formation, after which a cooling rate of 5 °C min^{-1} was used. Unless otherwise noted, all of the above procedures occurred in static air atmosphere. The electrode was weighed before and after the deposition process to estimate the oxide thickness [35]. The PbO_2 coatings were electrodeposited at 65 °C to obtain a 50 mg cm^{-2} PbO_2 film, i.e., 40.33C cm^{-2}, calculated assuming 100% efficiency by Faraday's law. The electrolytic bath contained 0.1 mol L^{-1} lead nitrate (Vetec), 1.0 mol L^{-1} nitric acid (Synth) and 1.0 g L^{-1} sodium dodecyl sulphate (Vetec), adapted from Aquino et al. [36]. For Bi-doped PbO_2 electrodeposition, 0.05 mol L^{-1} bismuth nitrate (Vetec) was added to the last electrolytic bath. The electrodeposition assays were performed at 5, 10, 15, 25 and 50 mA cm^{-2} current densities for PbO_2 and Bi-doped PbO_2, but the most uniform and homogeneous coatings for the two electrode surfaces were only obtained at 5 mA cm^{-2}. Thus, the electrodeposition of all films used in these experiments was carried out at 5 mA cm^{-2} during 3 hours 21 minutes for obtaining of 80 μm coatings. Caution was necessary to remove the electrode from the plating solution to avoid the cracking of the coating due to the difference of temperature. The electrodeposits were characterised by EDX, SEM, XRD and, to evaluate the electrochemical relative roughness factor (R_f) of the films, cyclic voltammetry. To compare the electrode lifetimes, accelerated corrosion experiments on films were carried out. Using similar approach utilized by Andrade et al. [26], a current density of 1 A cm^{-2} was applied on the electrodes immersed in 0.5 mol L^{-1} $HClO_4$ at 50 °C and during 1400 min. The values of open circuit potential (OCP) were measured at each 200 min. The current density and the bath temperature were increased in relation to experiment described by aforementioned authors in order to reduce the experimental time until to observe the film failure.

2.4. Electrochemical oxidation assays

Before beginning electrodegradation experiments, a linear voltammetry analysis was performed to investigate the electroactivity of TBC, with measurements at room temperature in 0.01 mol L^{-1} $NaClO_4$ (Aldrich, 98%) and in 12.5 mg L^{-1} TBC, prepared by serial dilution in 0.01 mol L^{-1} $NaClO_4$.

The initial concentration of TBC was selected as 12.5 mg L^{-1} and all anodic oxidation assays were performed under galvanostatic conditions at 27 °C, with applied current densities of 20, 30, 40 and 50 mA cm^{-2}, in 80 mL of 0.01 mol L^{-1} $NaClO_4$. This electrolyte was carefully chosen because it does not suffer electrochemical oxidation, i.e, it does not generate other oxidant species that could change the mechanism of degradation of the TBC [1]. During the experiments, samples were collected from the electrochemical cell at certain time intervals for analysis by TOC measurements and by UV–vis spectrophotometry at characteristic absorption wavelengths to follow the evolution of molecular absorption.

3. Results and discussion

3.1. EDX, SEM and XRD characterisation

The films were characterised by EDX, with the results revealing that the interlayer SnO_2–Sn_2O_5 had 12% of Sb relative to Sn and that Bi-doped PbO_2 has 8% of Bi relative to Pb. SEM images of the Ti/SnO_2–Sn_2O_5, PbO_2 and Bi-doped PbO_2 films are shown in Fig. 1.

As shown in Fig. 1A, the Ti/SnO_2–Sn_2O_5 electrode surface exhibited a typical cracked-mud structure, which is common to

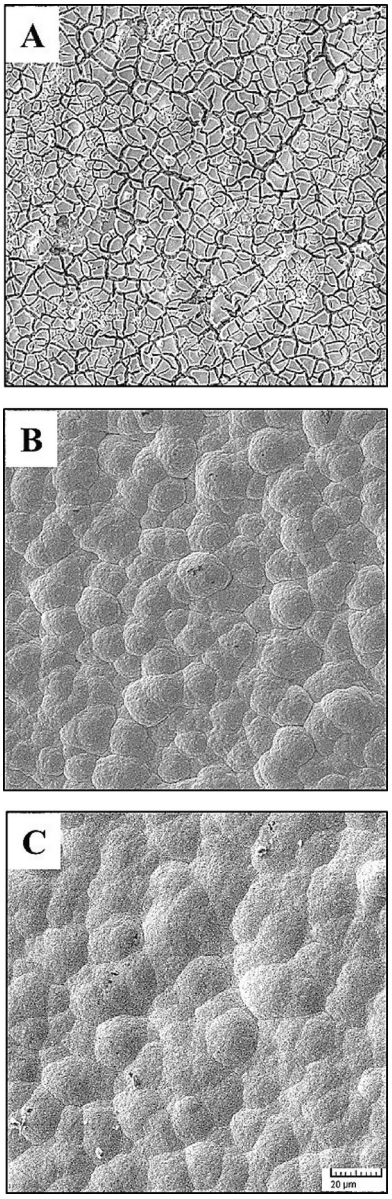

Fig. 1. SEM images of the coatings. A) Sb-doped SnO_2 produced by thermal decomposition. B) PbO_2 and C) Bi-doped PbO_2, both electrodeposited at 5 mA cm^{-2} and 65 °C on the Ti/Sb-doped SnO_2 substrate.

thermally prepared coatings [35,37,38]. This morphology is consistent with some previously published works, e.g., Montilla et al. [35]. SnO_2–Sn_2O_5 is sometimes reported [36,39,40] as having chemical and electrochemical stability. It may effectively slow the diffusion of nascent oxygen towards the matrix and prevent the formation of a TiO_2-insulated layer on the Ti substrate, which is very important to improve the adherence of the PbO_2 films and the lifetime and electrocatalytic activity of the electrodes. Fig. 1B and 1C show SEM images of the Ti/SnO_2–Sn_2O_5/PbO_2 and Ti/SnO_2–Sn_2O_5/Bi-doped PbO_2 electrode surfaces. These two SEM images show that these films have similar globular morphologies, which are not commonly reported in the literature for electrodeposited PbO_2 films in inorganic medium [25]. These PbO_2 coatings consist of larger grains [25] compared with those formed at slower electrodeposition rates (applied current density of 5 mA cm^{-2}). This procedure has been found to reduce the number of defects in the films [36]. In addition, the insertion of Bi does not cause a visible change on morphology of the PbO_2 films.

Usually, the quantities of α- and β-PbO_2 forms are evaluated from X-ray diffractograms using the area of the characteristic peaks (integration of the peaks corrected for background), but this methodology only gives a semi-quantitative evaluation [25,41–43]. Munichandraiah [44] calculated the percentages of the two forms in deposits by a mathematical expression adapted from Dodson [45], using the most intense lines in the XRD spectra and mathematically comparing them with the calibrated relationship between the XRD line intensities and the mixture compositions [44].

However, the form and crystallographic orientation of the electrodeposited PbO_2 are very different from those of the PbO_2 obtained using non-electrochemical methodologies and are dependent on many parameters, such as the substrate nature and its pre-treatment, the electrochemical bath composition (pH, concentration and presence of additive or doping ions), the temperature and the applied potential or current density [25,42]. Therefore, the calculation of the ratio of α and β forms, through X-ray data processing using the methodologies mentioned above, cannot lead to accurate results. Thus, we used the Rietveld refinement methodology to estimate this value and to determine other crystallographic parameters for PbO_2 films.

In Rietveld refinement, the theoretical peak profiles are fitted to converge with the measured profiles through a least-squares approach, which presents several advantages over conventional quantitative analysis methods, including the use of pattern-fitting algorithms. All lines of each crystallographic phase were explicitly considered, even the overlapping lines. Thus, it was not necessary to decompose the patterns into separate Bragg peaks. The use of all reflections in a pattern, rather than just the most intense ones, minimised the uncertainty in the derived weight fractions and the effects of preferred orientation, primary extinction, and nonlinear detection systems [46].

In the literature [47,48], the data from structural refinements are generally checked by quality algorithms or R-factors (R_p, R_{wp}, R_{Bragg} and χ^2); however, the difference between the measured and calculated patterns can also be considered a way to verify the success of the refinement. Thus, in the following Rietveld refinements, the measured diffraction patterns of PbO_2 and Bi-doped PbO_2 films were well adjusted to the standard data obtained from ICSD, collection code numbers 23292 (β-PbO_2) and 415268 (α-PbO_2) [34], without any bismuth oxide secondary phases. The parameters of the refinements and the estimated ratio between α and β forms can be observed in Fig. 2A and B and in Table 1.

Fig. 2A and B shows the agreement between the experimental and calculated XRD patterns, thus proving the accuracy of the structural refinements for PbO_2 and Bi-doped PbO_2 films. This can be also observed from the data in Table 1; a structural refinement R_{wp} value of less than 10% for medium complex phases (tetragonal and orthorhombic phases) is commonly acceptable. The low values for R_{Bragg} and χ^2 are also indicative of the accuracy of the obtained refinement results [47]. As predicted, the high temperature and the acid medium favoured the β-phase formation: PbO_2 and Bi-doped PbO_2 films only showed a level of 1 and 2% of the α-phase, respectively. In comparison with the PbO_2 lattice parameters, the slightly larger values observed for the Bi-doped film (Table 1) are consistent with the fact of the majority of the Bi-ions doping be present as Bi(V), as discussed by Popovic et al. [49]. As observed in Table 1, the insertion of Bi-ions increased the values of the lattice parameters and decreased the size of the coherent domain of the crystal (D). This was attributed to the formation of Bi_2O_5 during the electrodeposition process, which changed the nucleation and growth of the crystal in the film. The small D values favoured the formation of a large specific area, which is one of the most important factors influencing the catalytic activities [50]. The preferential orientation of the crystals was another crystallographic characteristic that was changed by doping of the PbO_2. For better visualisation, Fig. 3A compares the diffraction patterns of the films

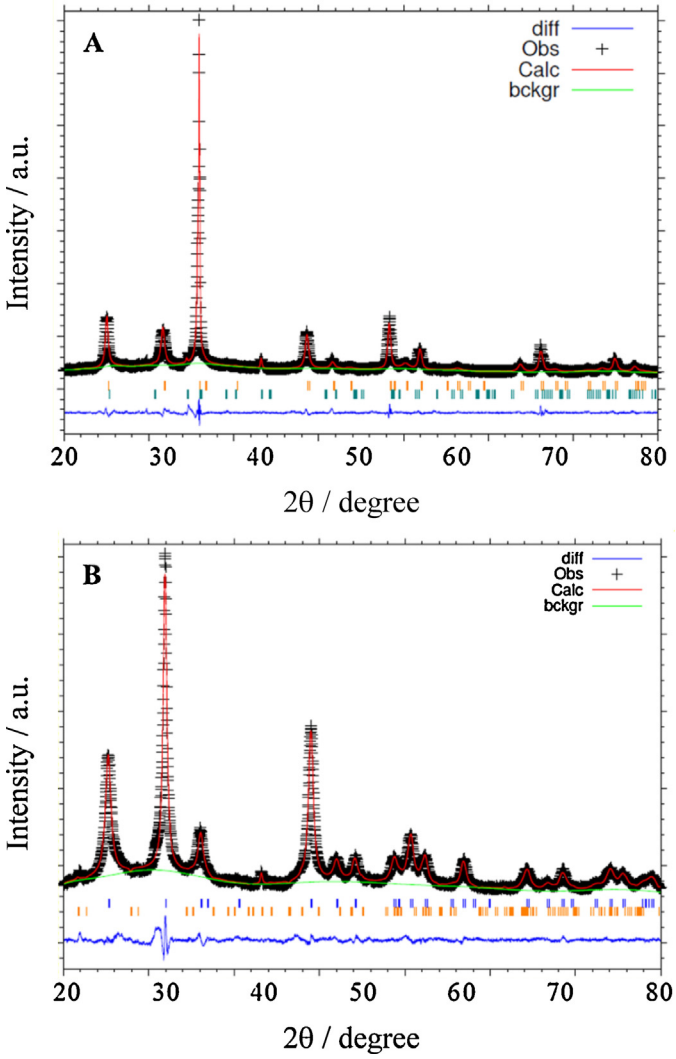

Fig. 2. Calculated X-ray diffraction patterns of A) Bi-doped PbO_2 and B) PbO_2, using Rietveld refinement. For an interpretation of the colours used in this figure, the reader is referred to the web version of the article.

Table 1
Rietveld refinement (RR) parameters, approximated phase content, cell parameters and size of the coherent domain of the crystal (D) for the PbO_2 and Bi-doped PbO_2 coatings.

	RR parameters				Phase content (%)	Cell parameters of the β-phase (pm)	D (nm)*
Film	R_p (%)	R_{wp} (%)	R_{bragg} (%)	χ^2			
PbO_2	2.33	3.12	9.95	3.880	Beta: 99% Alfa: 1%	a = b = 4.965 c = 3.383	14.14
Bi-doped PbO_2	3.40	4.53	1.76	5.983	Beta: 98% Alfa: 2%	a = b = 4.990 c = 3.403	6.50

* Calculated from peak (101).

(Bi-doped PbO_2 and PbO_2) with non-preferentially oriented powder β-PbO_2 (ICSD Collection Code 23292 [34]).

It can be clearly observed that there is different texturing in the obtained films. The doping did not disturb the rutile structure of the β-PbO_2; however, the Bi-doped β- PbO_2 film showed a well-defined texturing in the direction of the (200) plane, where the diffraction phenomena promoted by parallel planes are intensified and the ones promoted by perpendicular planes are suppressed; *i.e.*, this film grew with the (200) plane preferentially oriented parallel to the substrate. This effect has been described by other authors [25,51]. A detached texturing phenomenon was not observed in PbO_2 films. The lattice parameters (Table 1) and atomic positions obtained by Rietveld refinement were used in the Diamond Crystal and Molecular Structure Visualisation program (Version 3.2i for Windows) [52] to model the unit cell of the Bi-doped film. Thus, Fig. 3B shows the representation of the Bi-doped unit cell and the texturisation plane.

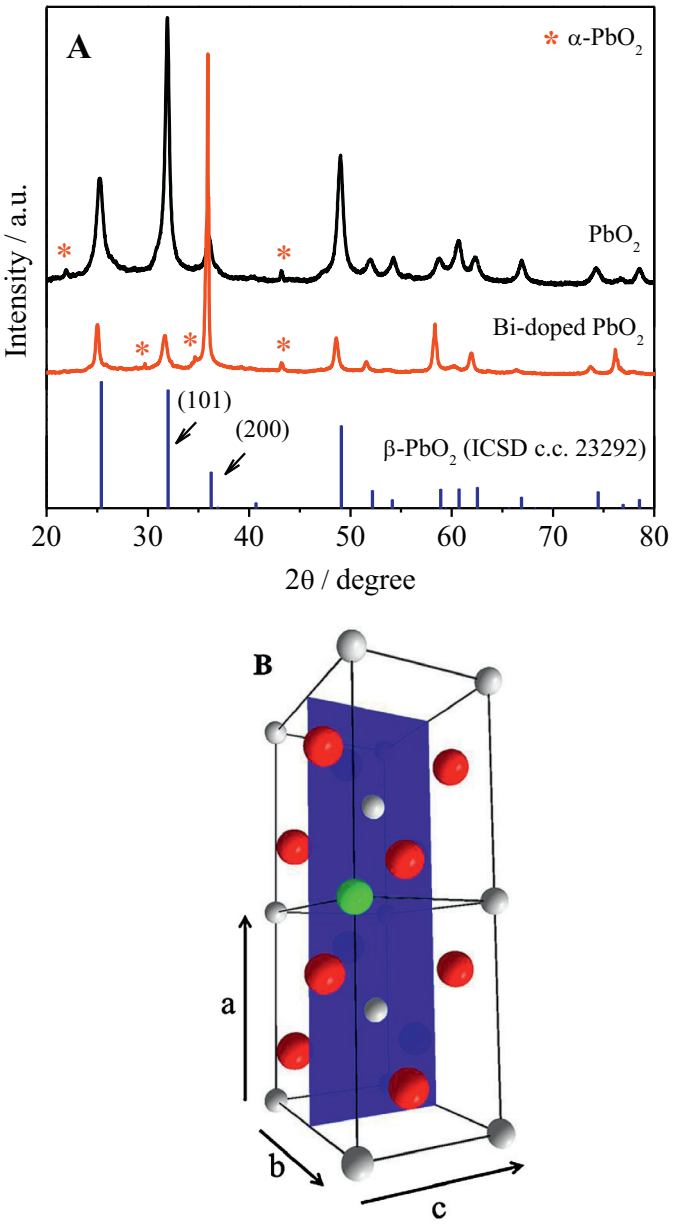

Fig. 3. A) XRD patterns corresponding to Powder Patterns from the ICSD, Collection Code 23292 (β-PbO_2) and to the Bi-doped PbO_2 and PbO_2 films. B) Unit cell of the Bi-doped PbO_2 film, in which the red atom is oxygen (2^-), the grey atom is lead (4^+), the green atom is bismuth and the blue plane is (200). For an interpretation of the colours used in this figure, the reader is referred to the web version of the article.

3.2. Electrochemical characterisation

To estimate the electrochemical relative roughness factor, R_f [53], an electrochemical characterisation of the PbO_2 and Bi-doped PbO_2 films by cyclic voltammetry, which was performed in the potential window of the double layer capacitance region with different scan rates. Because the electrode was composed of conducing oxide, there was a linear dependence between the double layer charging current and the scan rate, with the slope closely related to the interfacial electrode/solution capacitance. From the methodology described by Ciríaco et al. [6], this experimentally obtained capacitance, normalised by the geometric area of the electrode, was compared to capacitance of an oxide with a smooth surface (60 μF cm^{-2} [53]), resulting in the R_f value. The applied equation described by Ciríaco et al. [6] can be seen below:

$$R_f = \frac{C_{PbO_2}}{60}$$

where C_{PbO2} is the normalized capacitance of the oxide/solution interface and 60 μF cm^{-2} is the capacitance of a oxide with a smooth surface.

Thus, the R_f values were calculated for both electrodes. The value for PbO_2 was 44, while that for Bi-doped PbO_2 was 186, suggesting that the Bi-doped PbO_2 films were four times rougher than the PbO_2 films. The cyclic voltammograms of theses studies can be seen in Supplementary Information (Fig. S1). These data were consistent with the size of the coherent domain of the crystal previously determined, with the Bi-doped PbO_2 showing a larger specific area than PbO_2.

Another electrochemical characterization carried out to compare those electrodes was the accelerated corrosion. For this, it was used more aggressive condition than used by Andrade et al. [26] in order to reduce the experimental time until to observe the film failure. Current density of 1 A cm^{-2} was applied on the electrodes immersed in 0.5 mol L^{-1} $HClO_4$ at 50 °C. Open circuit potential (OCP) was measured at each 200 min and the electrode peeling was also accompanied during this time. Before to measure this

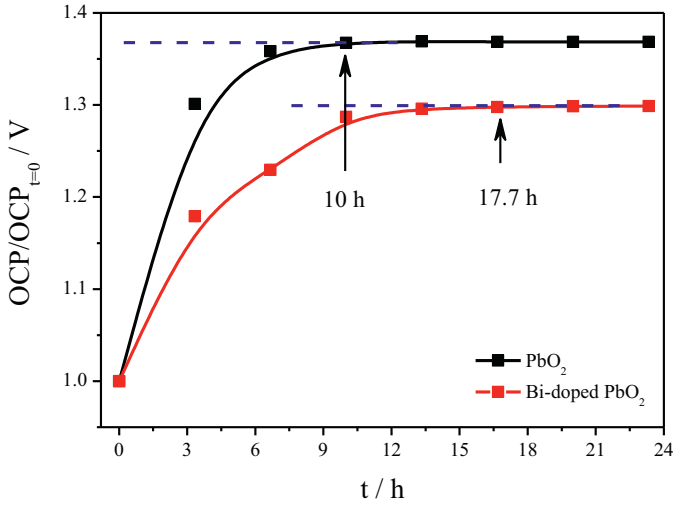

Fig. 4. Open circuit potential (OCP) as function of the time for accelerated corrosion studies carried out in 0.5 mol L^{-1} $HClO_4$ at 50 °C applying 1 A cm^{-2}.

parameter, the system was resting at open circuit condition for 30 min. In Fig. 4, it can be seen the OCP as function of time.

3.3. Electrochemical degradation of tebuconazole

3.3.1. Effect of current density and anode material

Before the electrodegradation assays, linear voltammetry measurements were carried out on Ti/SnO_2–Sn_2O_5/Bi-doped PbO_2 in 0.01 mol L^{-1} $NaClO_4$ and in 0.01 mol L^{-1} $NaClO_4$ with 12.5 mg L^{-1} TBC, from 0.5 V to 1.7 V, to verify the electroactivity of the TBC molecule on the electrode surface. The linear voltammograms for these experiments can be seen in Fig. 5.

Degradation assays of 12.5 mg L^{-1} TBC solutions were performed using the Ti/SnO_2–Sn_2O_5/Bi-doped PbO_2 electrode at 20, 30, 40 and 50 mA cm^{-2} current densities. To monitor the evolution of the electrochemical degradation, UV–vis spectrophotometric analysis and TOC measurements were performed, with the results displayed as function of the electrolysis time in Fig. 6.

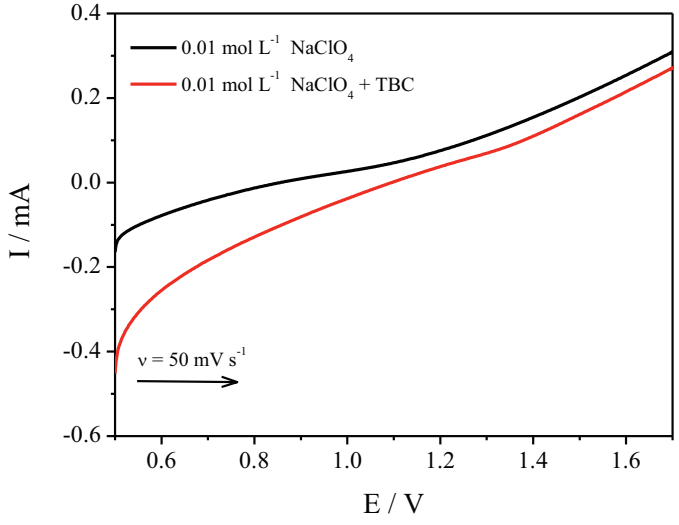

Fig. 5. Linear voltammograms on Ti/SnO_2–Sn_2O_5/Bi-doped PbO_2 in medium of 0.01 mol L^{-1} $NaClO_4$ (black line) and of 0.01 mol L^{-1} $NaClO_4$ with 12.5 mg L^{-1} TBC (red line), at 50 mV s^{-1}. (For interpretation of the references to colour in this figure legend, the reader is referred to the web version of this article.)

Fig. 6A shows the UV–vis spectra for TBC degradation using the Ti/SnO_2–Sn_2O_5/Bi-doped PbO_2 electrode at 40 mA cm^{-2} and 27 °C. The increasing absorbance at approximately 220 nm is most likely due to the formation of a secondary species, absorbing in the same TBC wavelength range. We think this increase could be associated

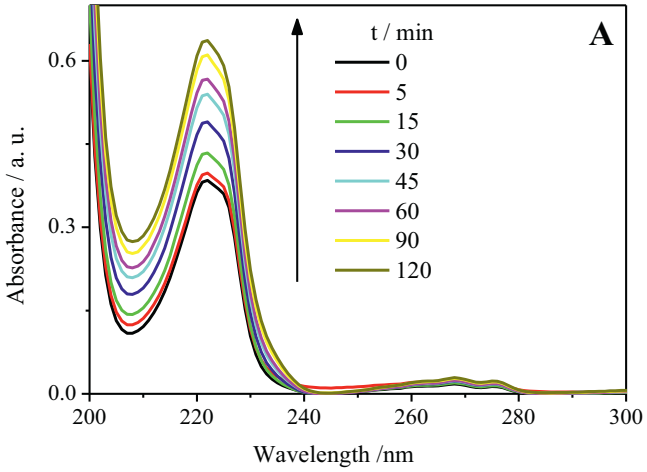

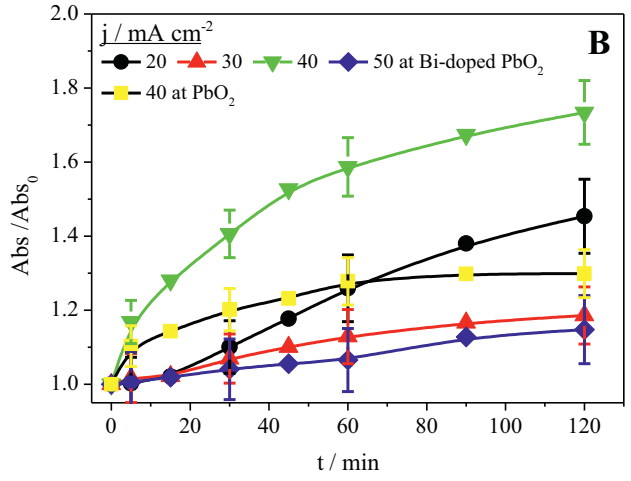

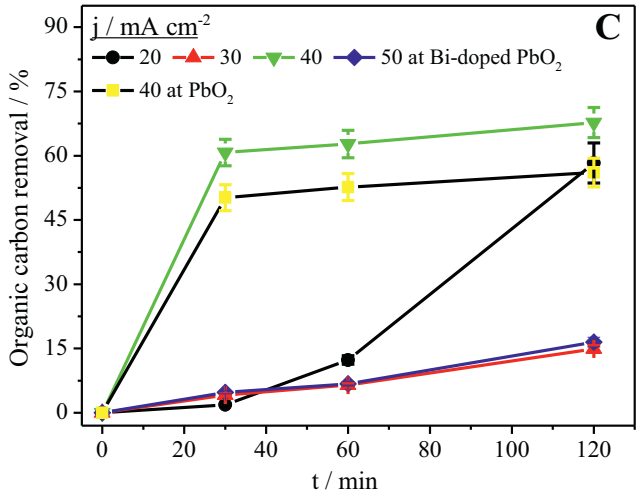

Fig. 6. A) UV–vis spectra for the electrodegradation assays with the Bi-doped PbO_2 anode at 40 mA cm^{-2}. Evolution of B) the absorbance at 220 nm and C) the total organic carbon degradation with time, for assays performed at different current densities) using Bi-doped PbO_2 and PbO_2 as anodes.

to nitrate ion formation during the electrolytic pesticide mineralisation. TBC includes nitrogen atoms, which could be converted to nitrate ions through attack by hydroxyl radicals, and the absorption range of these ions is very close to that of TBC [54,55].

Fig. 6B and C shows the relative evolution of the absorbance at approximately 220 nm and the organic carbon removal with electrochemical degradation for different applied current densities, respectively. Of the applied current densities, 40 mA cm^{-2} displayed the highest increase in the absorbance associated with TBC mineralisation and TOC removal. The electrodegradation assays were repeated under the same conditions with the Ti/SnO_2–Sn_2O_5/PbO_2 electrode to compare the doping effect. It can be observed from Fig. 6B and C that both the relative increase of the absorbance band and the TOC removal were higher for the Bi-doped PbO_2 electrode than for PbO_2. At 40 mA cm^{-2}, the TOC removal for the Bi-doped PbO_2 was of 68%, while it was only 56% for the PbO_2. These results clearly show that Bi doping of the PbO_2 coatings improved the mineralisation capacity of this electrode material. This catalytic enhancement can be result of an associated effect comprising the decreased size of the coherent domain of the crystal, the increased electrochemical roughness, the increased crystallographic preferential orientation and the proportioning of adsorption sites by the insertion of Bi ions. However the isolated effect of each one of this parameter is difficult of being taken in account.

3.3.2. Proposed tebuconazole oxidation pathway

The electrochemical oxidation mechanism was studied using HPLC-ESI/HRMS, the products were separated by HPLC and identified by its ESI–HRMS spectrum. The ESI–HR mass spectrum of each identified oxidation product and its fragmentation pathway can be observed in Supporting Information from Fig. S3–Fig. S11. Electrospray ionization mechanism associated to the high-resolution determination of the charge/mass of each fragment helped us to propose a good fragmentation pathway and to identify the formed product of the TBC electrooxidation. Thus, assuming that •OH is the major oxidising agent [1], like all AOP, and based on the spectra obtained from ESI–HRMS, it is possible to suggest the oxidation pathway for TBC on the Bi-doped PbO_2 anode (Scheme 1). In evaluating the molecular masses of the electrooxidation products, which were obtained via high-resolution MS, it was apparent that there were several •OH additions/substitutions on

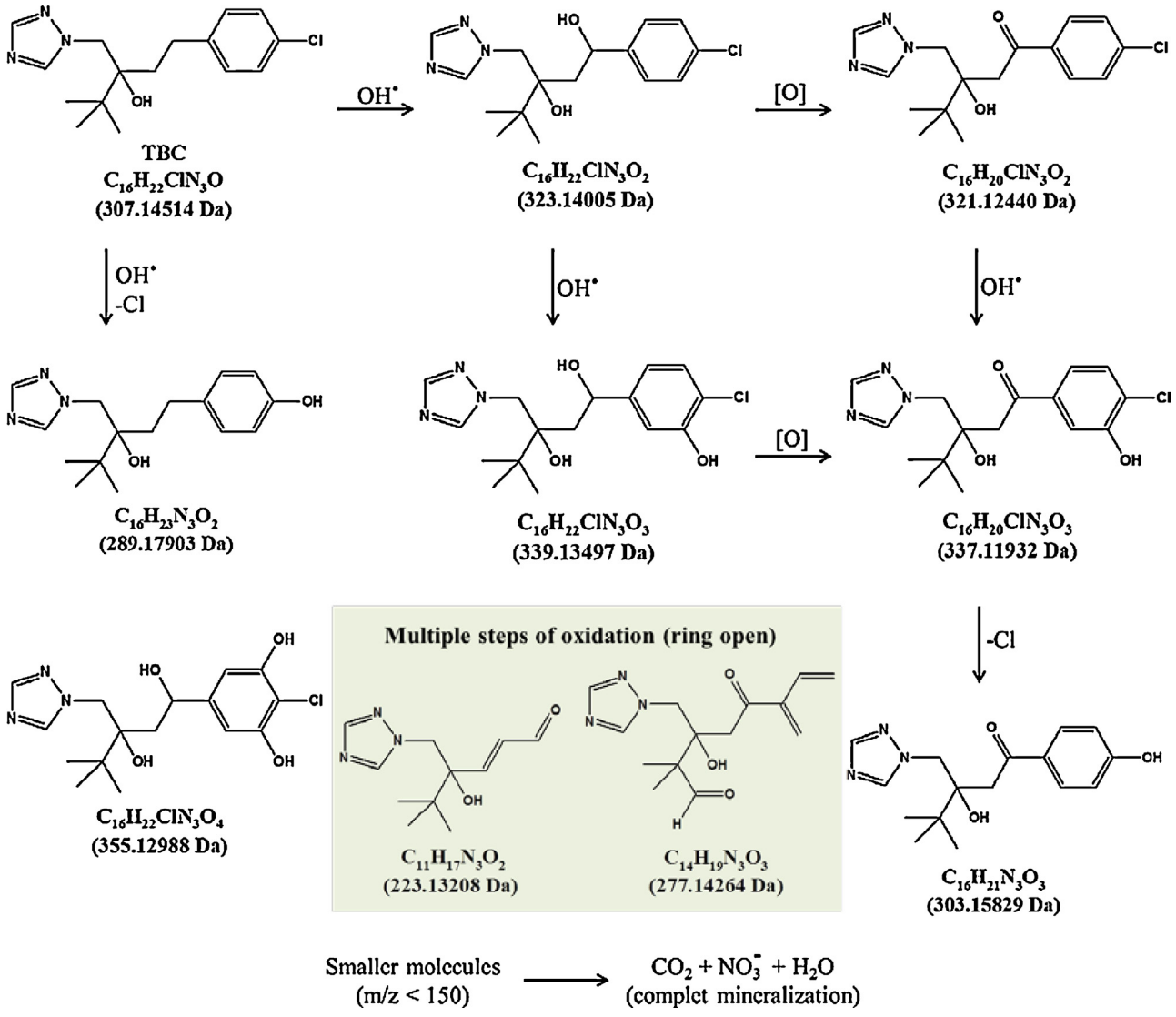

Scheme 1. Proposed electrodegradation pathway of tebuconazole.

phenyl groups, as evidenced by their consequent oxidation to ketones and by mono- and dihydroxylated phenyl rings (likely stemming from TBC). There was also evidence of Cl atom substitution by OH (resulting in two different dechlorinated products), ring opening due to multiple steps of TBC oxidations (resulting in two different products) and successive attacks by OH, leading to the formation of small molecules ($m/z < 150$). These molecules were mineralised, producing lower toxicity compounds, such CO_2, NO_3^- and H_2O. This mineralisation was verified by TOC analysis, where more than 50% of the organic compounds were converted to inorganic ones.

Calza et al. [20] identified more degradation products than the observed in this work; they verified that the photodegradation of the TCB using TiO_2 as catalyst produced twelve main products. In contrast, this present study observed the formation of nine main products of the electrodegradation of this compound, of which four were also observed in the aforementioned study; the compounds with mass 323.14005 Da, 321.12440 Da, 277.14264 Da and 223.13208 Da. They observed an isomer of the 223.13208 Da compound with hydroxyl linked to the aromatic ring, two different ring opening compounds and others. Thus, we conclude that the degradation of the TBC is depending on the method/catalyst, producing different intermediary products.

4. Conclusions

Ti/SnO_2–Sn_2O_5/PbO_2 and Ti/SnO_2–Sn_2O_5/Bi-doped PbO_2 were prepared and analysed by SEM, XRD (with Rietveld refinement), EDX and cyclic voltammetry. The Bi-doped PbO_2 film had 8% Bi, relative to Pb. This insertion of Bi ions in the PbO_2 structure did not cause a visible change in the morphology, which was globular. XRD analysis with Rietveld refinement demonstrated that the films were essentially single β-phase (with less than 2% composed of α-phase) and that the majority of the Bi-cations doping were present as Bi(V). Bi-doped film showed a well-defined texturing in the direction of the (2 0 0) plane, had smaller coherent domain of the crystal and was four times rougher than PbO_2, suggesting a large specific area [50]. From TOC analysis, it was possible to conclude that, among the current densities studied, the greatest organic carbon degradation took place at 40 mA cm^{-2}. In comparing both electrodes at the same current density, it was apparent that doping increases the oxidation power of the PbO_2 because the Bi-doped PbO_2 was responsible for 68% of the TOC removal, while the PbO_2 was responsible for 56%. HPLC-ESI/HRMS results allowed the identification of some oxidation products and the determination of the TBC oxidation pathway. Nine electrooxidation products were identified, resulting from the following: hydroxylation of the TBC phenyl group and its consequent oxidation to a ketone (including both mono- and dihydroxylated products), dechlorination (two different products), and oxidative ring opening (two different products). The scheme also demonstrates that the electrochemical oxidation of TBC using Bi-doped PbO_2 generates less toxic products than TBC, recommending this anode as an alternative material for the decontamination of wastewater.

Acknowledgements

The authors gratefully acknowledge Prof. Dr. Antonio A. Mozeto (*Laboratório de Biogeoquímica Ambiental*, DQ/UFSCar–São Carlos, SP, Brazil), by the TOC analysis, and Brazilian funding agencies FINEP,CNPq and CAPES (Funcap/23038.007973/2012-90) for the financial support. Lucas, F.W.S. and Mascaro, L.H, wish to thank São Paulo Research Foundation (FAPESP), grant 2012/10947-2.

Appendix A. Supplementary data

Supplementary data associated with this article can be found, in the online version, at http://dx.doi.org/10.1016/j.electacta.2014.12.062.

References

[1] M. Panizza, G. Cerisola, Direct and mediated anodic oxidation of organic pollutants, Chem. Rev. 109 (2009) 6541.
[2] Electrochemistry for the Environment, in: C. Comninellis, G. Chen (Eds.), Springer, New York, 2010.
[3] L.S. Andrade, L.A.M. Ruotolo, R.C. Rocha-Filho, N. Bocchi, S.R. Biaggio, J. Iniesta, V. García-Garcia, V. Montiel, On the performance of Fe and Fe, F doped Ti–Pt/PbO_2 electrodes in the electrooxidation of the Blue Reactive 19 dye in simulated textile wastewater, Chemosphere 66 (2007) 2035.
[4] K. Rajeshwar, J.G. Ibanez, G.M. Swain, Electrochemistry and the environment, J. Appl. Electrochem. 24 (1994) 1077.
[5] R.G. da Silva, S. Aquino Neto, A.R. de Andrade, Electrochemical degradation of reactive dyes at different DSA® compositions, J. Braz. Chem. Soc. 22 (2011) 126.
[6] L. Ciríaco, C. Anjo, J. Correia, M.J. Pacheco, A. Lopes, Electrochemical degradation of Ibuprofen on Ti/Pt/PbO_2 and Si/BDD electrodes, Electrochim. Acta 54 (2009) 1464.
[7] J. Wang, W. Sun, Z. Zhang, X. Zhang, R. Li, T. Ma, P. Zhang, Y. Li, Sonocatalytic degradation of methyl parathion in the presence of micron-sized and nano-sized rutile titanium dioxide catalysts and comparison of their sonocatalytic abilities, J. Mol. Catal. A: Chem. 272 (2007) 84.
[8] A. Zaleska, J. Hupka, Problem of disposal of unwanted pesticides deposited in concrete tombs, Waste Manage. Res. 17 (1999) 220.
[9] Food and Agriculture Organization of the United Nations, Tebuconazole (188). http://www.fao.org.
[10] C.W. Götz, C. Stamm, K. Fenner, H. Singer, M. Schärer, J. Hollender, Targeting aquatic microcontaminants for monitoring: exposure categorization and application to the Swiss situation, Environ. Sci. Pollut. Res. Int. 17 (2010) 341.
[11] N. Stamatis, D. Hela, I. Konstantinou, Occurrence and removal of fungicides in municipal sewage treatment plant, J. Hazard. Mater. 175 (2010) 829.
[12] J. Kreuger, Pesticides in stream water within an agricultural catchment in southern Sweden, 1990–1996, Sci. Total Environ. 216 (1998) 227.
[13] N. Berenzen, A. Lentzen-Godding, M. Probst, H. Schulz, R. Schulz, M. Liess, A comparison of predicted and measured levels of runoff-related pesticide concentrations in small lowland streams on a landscape level, Chemosphere 58 (2005) 683.
[14] J.-B. Baugros, B. Giroud, G. Dessalces, M.-F. Grenier-Loustalot, C. Cren-Olivé, Multiresidue analytical methods for the ultra-trace quantification of 33 priority substances present in the list of reach in real water samples, Anal. Chim. Acta 607 (2008) 191.
[15] N. Berenzen, S. Hümmer, M. Liess, R. Schulz, Pesticide peak discharge from wastewater treatment plants into streams during the main period of insecticide application: ecotoxicological evaluation in comparison to runoff, Bull. Environ. Contam. Toxicol. 70 (2003) 891.
[16] C. De Rossi, R. Bierl, J. Riefstahl, Organic pollutants in precipitation: monitoring of pesticides and polycyclic aromatic hydrocarbons in the region of Trier (Germany), Phys. Chem. Earth Parts A/B/C 28 (2003) 307.
[17] National Health Surveillance Agency. http://portal.anvisa.gov.br/wps/portal/anvisa-ingles.
[18] S. Navarro, J. Fenoll, N. Vela, E. Ruiz, G. Navarro, Photocatalytic degradation of eight pesticides in leaching water by use of ZnO under natural sunlight, J. Hazard. Mater. 172 (2009) 1303.
[19] T. de, H. Prestes, D. de, O. Gibbon, M.A. Lansarin, C.C. Moro, Degradação fotocatalítica do fungicida tebuconazole em solução aquosa, Quim. Nova 33 (2010) 798.
[20] P. Calza, S. Baudino, R. Aigotti, C. Baiocchi, P. Branca, E. Pelizzetti, High-performance liquid chromatographic/tandem mass spectrometric identification of the phototransformation products of tebuconazole on titanium dioxide, J. Mass Spectrom. 37 (2002) 566.
[21] F.L. Migliorini, N.A. Braga, S.A. Alves, M.R.V. Lanza, M. Baldan, N.G. Ferreira, Anodic oxidation of wastewater containing the Reactive Orange 16 Dye using heavily boron-doped diamond electrodes, J. Hazard. Mater. 192 (2011) 1683.
[22] M. Panizza, L. Ouattara, E. Baranova, C. Comninellis, DSA-type anode based on conductive porous p-silicon substrate, Electrochem. Commun. 5 (2003) 365.
[23] M. Zhou, L. Liu, Y. Jiao, Q. Wang, Q. Tan, Treatment of high-salinity reverse osmosis concentrate by electrochemical oxidation on BDD and DSA electrodes, Desalination 277 (2011) 201.
[24] C.R. Costa, C.M.R. Botta, E.L.G. Espindola, P. Olivi, Electrochemical treatment of tannery wastewater using DSA electrodes, J. Hazard. Mater. 153 (2008) 616–627.
[25] X. Li, D. Pletcher, F.C. Walsh, Electrodeposited lead dioxide coatings, Chem. Soc. Rev. 40 (2011) 3879.
[26] L.S. Andrade, R.C. Rocha-Filho, N. Bocchi, S.R. Biaggio, J. Iniesta, V. García-Garcia, V. Montiel, Degradation of phenol using Co-and Co, F-doped PbO_2 anodes in electrochemical filter-press cells, J. Hazard. Mater. 153 (2008) 252.
[27] N. Chahmana, M. Matrakova, L. Zerroual, D. Pavlov, Influence of some metal ions on the structure and properties of doped β-PbO_2, J. Power Sources 191 (2009) 51.

[28] N.B. Tahar, A. Savall, Electrochemical degradation of phenol in aqueous solution on bismuth doped lead dioxide: a comparison of the activities of various electrode formulations, J. Appl. Electrochem. 29 (1999) 277.
[29] H. Liu, Y. Liu, C. Zhang, R. Shen, Electrocatalytic oxidation of nitrophenols in aqueous solution using modified PbO_2 electrodes, J. Appl. Electrochem. 38 (2007) 101.
[30] Y. Liu, H. Liu, J. Ma, X. Wang, Comparison of degradation mechanism of electrochemical oxidation of di- and tri-nitrophenols on Bi-doped lead dioxide electrode: Effect of the molecular structure, Appl. Catal. B: Environ. 91 (2009) 284.
[31] N.S. Gonçalves, J.A. Carvalho, Z.M. Lima, J.M. Sasaki, Size–strain study of NiO nanoparticles by X-ray powder diffraction line broadening, Mater. Lett. 72 (2012) 36.
[32] R.A. Young, The Rietveld Method, Oxford University Press, London, 1995.
[33] A.C. Larson, R.B. von Dreele, General Structure Analysis System (GSAS), Los Alamos National Laboratory Report LAUR 8 (1994) 6–748.
[34] [34] Inorganic Crystal Structure Database. http://www.fiz-karlsruhe.de/icsd.html.
[35] F. Montilla, E. Morallón, A. De Battisti, S. Barison, S. Daolio, J.L. Vázquez, Preparation and Characterization of Antimony-Doped Tin Dioxide Electrodes. 3. XPS and SIMS Characterization, J. Phys. Chem. B 108 (2004) 15976.
[36] J.M. Aquino, K. Irikura, R.C. Rocha-Filho, N. Bocchi, S.R. Biaggio, A comparison of electrodeposited Ti/β-PbO_2 and Ti–Pt/β-PbO_2 anodes in the electrochemical degradation of the direct yellow 86 dye, Quim. Nova 33 (2010) 2124.
[37] L.S. Andrade, R.C. Rocha-Filho, N. Bocchi, S.R. Biaggio, Estudo de efeito dos sais precursores sobre as propriedades eletrocatalíticas de eletrodos de Ti–SnO_2/Sb preparados por decomposição térmica, Quim. Nova 27 (2004) 866.
[38] A.P. Rizzato, L. Broussous, C.V. Santilli, S.H. Pulcinelli, A.F. Craievich, Structure of SnO_2 alcosols and films prepared by sol-gel dip coating, J. Non. Cryst. Solids 284 (2001) 61.
[39] S. Song, J. Fan, Z. He, L. Zhan, Z. Liu, J. Chen, X. Xu, Electrochemical degradation of azo dye C.I. Reactive Red 195 by anodic oxidation on Ti/SnO_2–Sb/PbO_2 electrodes, Electrochim. Acta 55 (2010) 3606.
[40] S. Song, L. Zhan, Z. He, L. Lin, J. Tu, Z. Zhang, J. Chen, L. Xu, Mechanism of the anodic oxidation of 4-chloro-3-methyl phenol in aqueous solution using Ti/SnO_2–Sb/PbO_2 electrodes, J. Hazard. Mater. 175 (2010) 614.
[41] I. Petersson, E. Ahlberg, B. Berghult, Parameters influencing the ratio between electrochemically formed α- and β-PbO_2, J. Power Sources 76 (1998) 98.
[42] D. Devilliers, M.T. Dinh Thi, E. Mahé, V. Dauriac, N. Lequeux, Electroanalytical investigations on electrodeposited lead dioxide, J. Electroanal. Chem. 573 (2004) 227.
[43] S. Abaci, K. Pekmez, T. Hökelek, A. Yildiz, Investigation of some parameters influencing electrocrystallisation of PbO_2, J. Power Sources 88 (2000) 232.
[44] N. Munichandraiah, Physicochemical properties of electrodeposited β-lead dioxide: effect of deposition current density, J. Appl. Electrochem. 22 (1992) 825.
[45] V.H. Dodson, Some important factors that influence the composition of the positive plate material in the lead-acid battery, J. Electrochem. Soc. 108 (1961) 401.
[46] M. Ferrari, L. Lutterotti, Method for the simultaneous determination of anisotropic residual stresses and texture by x-ray diffraction, J. Appl. Phys. 76 (1994) 7246.
[47] L.S. Cavalcante, V.M. Longo, J.C. Sczancoski, M.A.P. Almeida, A.A. Batista, J.A. Varela, M.O. Orlandi, E. Longo, M.S. Li, Electronic structure, growth mechanism and photoluminescence of $CaWO_4$ crystals, Cryst. Eng. Comm. 14 (2012) 853.
[48] I. Lonardelli, H.R. Wenk, L. Lutterotti, M. Goodwin, Texture analysis from synchrotron diffraction images with the Rietveld method: dinosaur tendon and salmon scale, J. Synchrotron Radiat. 12 (2005) 354.
[49] N.D. Popovic, J.A. Cox, D.C. Johnson, Electrocatalytic function of Bi(V) sites in heavily-doped PbO_2-film electrodes applied for anodic detection of selected sulfur compounds, J. Electroanal. Chem. 455 (1998) 153.
[50] Y. Liu, H. Liu, Comparative studies on the electrocatalytic properties of modified PbO_2 anodes, Electrochim. Acta 53 (2008) 5077.
[51] I.-H. Yeo, Electrocatalysis of anodic oxygen transfer reactions: comparison of structural data with electrocatalytic phenomena for bismuth-doped lead dioxide, J. Electrochem. Soc. 136 (1989) 1395.
[52] K. Brandenburg, Diamond Crystal and Molecular Structure Visualization, 2012. Downloaded from: http://www.crystalimpact.com/diam.
[53] S. Levine, A.L. Smith, Theory of the differential capacity of the oxide/aqueous electrolyte interface, Discuss. Faraday Soc. 52 (1971) 290.
[54] B. Roig, O. Thomas, UV spectrophotometry:a powerful tool for environmental measurement, Manag. Environ. Qual. Int. J. 14 (2003) 398.
[55] M.A. Ferree, R.D. Shannon, Evaluation of a second derivative UV/visible spectroscopy technique for nitrate and total nitrogen analysis of wastewater samples, Water Res. 35 (2001) 327.